

Contents lists available at ScienceDirect

# Petroleum Science

journal homepage: www.keaipublishing.com/en/journals/petroleum-science



# Original Paper

# Study on the performance variation and failure mechanism of natural gas pipeline under the action of water failure



Hai-Liang Nie <sup>a, \*</sup>, Zhi-Yong Wang <sup>b</sup>, Chen Chen <sup>c</sup>, Wei Dang <sup>a</sup>, Sen Zhao <sup>a</sup>, Jun-Jie Ren <sup>a</sup>, Xiao-Bin Liang <sup>a</sup>, Ke Wang <sup>a</sup>, Wei-Feng Ma <sup>a</sup>

- <sup>a</sup> Institute of Safety Assessment and Integrity, State Key Laboratory of Oil and Gas Equipment, CNPC Tubular Goods Research Institute, Xi'an, 710077, Shaanxi, China
- <sup>b</sup> Shanxi Guohua Energy Co., LTD, Taiyuan, 030000, Shanxi, China
- <sup>c</sup> Shaanxi Provincial Land Engineering Construction Group, Xi'an, 710075, Shaanxi, China

#### ARTICLE INFO

#### Article history: Received 25 August 2024 Received in revised form 27 November 2024 Accepted 20 March 2025 Available online 21 March 2025

Edited by Teng Zhu and Jia-Jia Fei

Keywords:
Water damage
River crossing
Natural gas pipeline
Performance variation rule
Failure mechanism

#### ABSTRACT

Water-induced disasters in long-distance pipelines are prevalent geological hazards, characterized by their frequency and widespread distribution. The complexity of factors contributing to pipeline damage in practical engineering poses a significant challenge for analysis using solely theoretical models. This study systematically reveals the cross-scale failure mechanism of long-distance pipelines under hydrodynamic impact through the combination of multi-scale experimental representation and theoretical modeling. Employing a combination of macroscopic measurements, advanced material testing of residual samples from failed pipelines, and consideration of operational conditions and environmental factors, the failure modes is systematically analyzed. The findings reveal that under the vibrations induced by water impulses, the pipe material exhibits a pronounced ratchet effect, leading to an 8.92% reduction in elongation at break. Furthermore, the Bauschinger effect is observed, resulting in a 2.95% decrease in yield strength. Cyclic hardening significantly diminishes the impact toughness of the weld by 22.2%. Notably, at high vibration frequencies of approximately 18.98 Hz, the stress concentration in the girth weld near the axial midpoint of the pipe section initiates cracking, ultimately leading to failure under the alternating load generated by the oscillation. This study provides valuable insights into the scientific understanding of pipeline failure mechanisms under water impact, contributing to the development of more robust and resilient pipeline systems.

© 2025 The Authors. Publishing services by Elsevier B.V. on behalf of KeAi Communications Co. Ltd. This is an open access article under the CC BY-NC-ND license (http://creativecommons.org/licenses/by-nc-nd/

4.0/).

#### 1. Introduction

As one of the five major transportation industries, pipeline transportation is the most economical and reasonable mode for transporting oil and natural gas. Due to the inflammable, explosive, and toxic characteristics of oil and natural gas, the safe operation of pipelines is crucial.

Long-distance oil and gas pipelines often traverse complex areas with varying hydrogeology and climatic environments, making them susceptible to various natural geological disasters. The variability in geological environmental conditions along the pipeline and the dynamic geological processes, both internal and external,

\* Corresponding author. E-mail address; niehailiang88@163.com (H.-L. Nie). contribute to the prevalence of geological disasters, including water damage. Water-related disasters are common in long-distance pipelines and represent one of the most frequent and widespread types of geological disasters. Based on survey data from the Oil and Gas Construction Quality Inspection Bureau of the former Soviet Union, 37 underwater pipeline crossing accidents occurred in the country during the 1990s (Xian, 2002). For instance, the Shiting River crossing section of the China Lancheng Pipeline was severely damaged by a once-in-a-century rainstorm in northwest Sichuan, leading to significant pipeline water damage (Zhang et al., 2015). Hence, many countries and societies have recognized the importance of addressing pipeline flood damage in recent years.

Regarding the interaction between water flow and pipeline, as early as 1987, an empirical pipe-soil interaction model was introduced, followed by an energy-based pipe-soil interaction model in 1989, which primarily examined the relationship between pipeline

erosion and instability (Hale et al., 1991). Based on the flow field simulation, Zhang et al. (2006) analyzed the stress form and source of the pipeline under the action of water flow, providing a mechanical model to investigate the process and cause of the pipeline water damage. Regarding pipeline vibration, Choi and Haun (1994) implemented the Rayleigh method to calculate the fundamental frequency of the pipeline span under residual tension and spaninduced moments, presenting a straightforward analytical approach applicable to river crossing pipelines of various sizes and water depths. Lu et al. (2002) derived partial differential equations for the vibration of suspended pipeline and proposed the iterative calculation method, with results validated against experimental measurements. When subjected to water scour, the pipeline experiences periodic alternating loads, resulting in deformation behaviors such as the ratchet effect (Paul et al., 2011a, b, c), Bauschenger effect (Bauschinger, 1881), and cyclic hardening (Krolo et al. 2016), which affect the structural performance. A large number of laboratory tests (Paul et al., 2011a, b, c; Lin et al., 2013; Xie et al., 2019; Guo et al., 2013, 2020; Wang et al., 2020) have shown that cyclic loading significantly deteriorates the mechanical properties of various materials, resulting in the reduction of the service life of the structure. In addition, finite element simulation and wide plate tensile test (Li et al., 2021) shown that external loads cause severe stress concentrations at the girth welds with misalignment defects, which makes these welds particularly susceptible to fracture in pipelines impacted by water flow is more likely to start from the girth welds with misalignment defect to fracture. Accordingly, previous research studied the structural response of pipelines under water flow impact through theoretical analysis, finite element simulation, or mechanical tests, rarely verified by actual engineering cases. However, pipeline water failures are often more complex with additional influencing factors. Therefore, a comprehensive analysis of the causes of pipeline failures is necessary based on actual operating conditions.

In the context of a specific water pipeline failure incident, this study presents an array of macroscopic measurements alongside extensive physical and chemical performance assessments of residual samples gathered directly from the site of the failed pipeline. Employing advanced materials science analysis techniques, notably Scanning Electron Microscopy (SEM) and Energy Dispersive Spectroscopy (EDS), the study delves into the microstructural and chemical attributes of the samples. Additionally, with consideration of the pipeline's operational parameters and service environment, the research scientifically investigates the mechanisms of deformation failure and the root causes of pipeline failures resulting from water flow in practical engineering scenarios. Through a comparative analysis that integrates mechanical models with empirical data, the study elucidates the intricate interplay between hydrodynamic forces and pipeline material characteristics, thereby offering a scientifically valuable case study for the analysis of water pipeline failures.

## 2. Background of the failed pipe

# 2.1. Failure process

The failure pipe section is directly buried beneath the riverbed pipeline. Due to long-term, extremely heavy rainfall, water erosion occurs in the riverbed, leading to soil loss and causing the crossing pipe to become exposed and suspended, as depicted in Fig. 1. The exposed length of the pipe section is approximately 40 m. The pipe material is L360, the diameter is 273 mm, the wall thickness is 7.1 mm, the design pressure is 4.0 MPa, and the anti-corrosion layer is 3 PE. The pipe employs straight seam resistance welding and features seven welding joints in the water-flushing area. The pipe



Fig. 1. Exposed pipe section after rain erosion.

section has remained in a state of shutdown following water damage. Approximately three months after exposure, the pipe section broke under water erosion at the girth weld near the center point of the suspended span pipe axis.

#### 2.2. Sampling situation

The sampling scheme for field pipe cutting is depicted in Fig. 2. Specimens No.1 and No.4 were taken from the far end of the fracture, each containing an unbroken girth weld. Specimens No.2 and No.3 are pipe segments on both sides of the fracture.

#### 2.3. Sample macro analysis and size measurement

Fig. 3 illustrates the failed pipe segment captured on-site, comprising four pipe segments, each 2 m in length. The anticorrosion layers on pipe segments No.1, No.2, and No.4 were stripped due to water damage, while the anti-corrosion layer on pipe segment No.3 retains the residual 3 PE layer not stripped at 200 mm from the fracture and extends axially about 300 mm.

The fracture in sample pipe No.2 was observed macroscopically. The fracture between 11:30 and 12:30 was flat and line-free; the fracture between 1:30 and 6:00 exhibited a pronounced crack expansion herringbone pattern, and the fracture was sharp and uneven; the fracture surface between 6:00 and 11:30 was uneven, with many sharp edges and corners. Step-like tear marks were present in the fracture at 6:00.

Radiographic examination of girth welds in sections No.1 and No.4 revealed no unqualified weld defects.

# 3. Experiment process

Samples from the straight pipe section, girth weld, fracture, and fracture edge of the pipe body were analyzed for their chemical composition, tensile properties, Charpy impact properties, and metallographic properties. The experimental process of this study is shown in Fig. 4.

#### 3.1. Sampling location

(1) Straight pipe body and straight weld (Specimen No.4)

Based on the Chinese standard GB/T 9711.1-1997 (SAC, 1997),

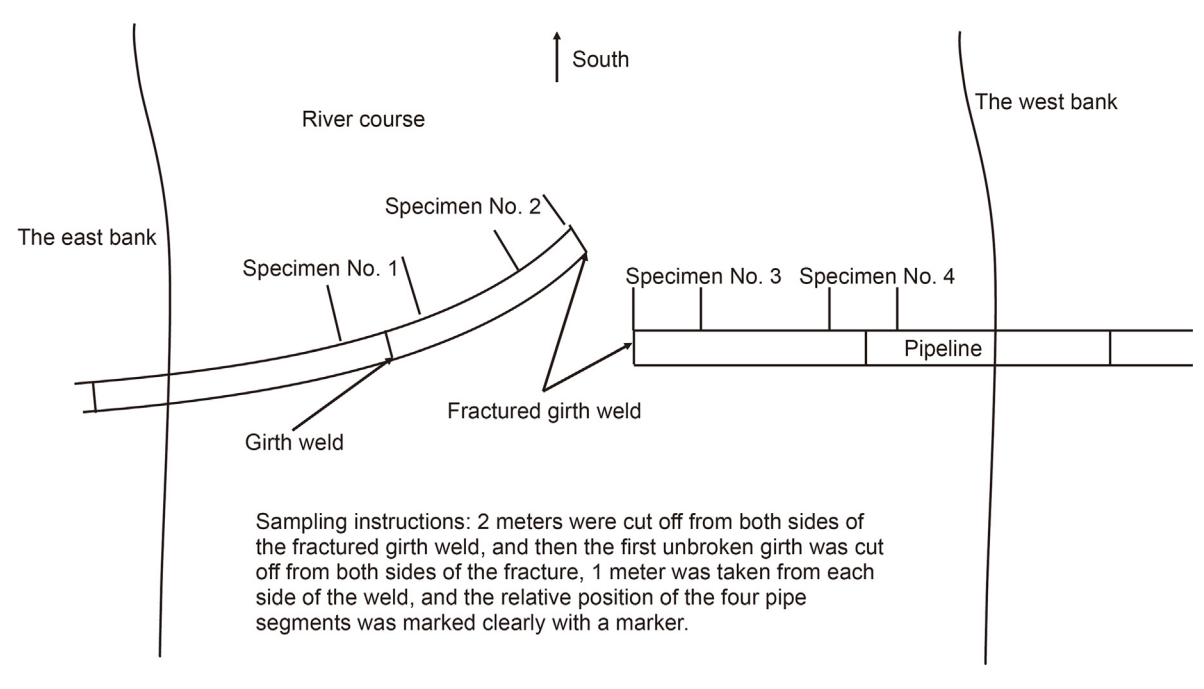


Fig. 2. Sampling scheme of cut pipe.



Fig. 3. Photo of sample pipe.

chemical composition, tensile properties, and Charpy impact properties of the base material of pipe section No.4 were sampled, and tensile properties, Charpy impact properties, metallographic properties, and bending properties of the straight weld were examined. The sampling position on pipe section No.4 is illustrated in Fig. 5(a).

(2) Pipe body and straight weld at fracture edge (Specimen No.3)

The pipe body and straight weld at the edge of the fracture were sampled and analyzed. The sampling position is shown in Fig. 5(b).

## (3) Girth weld

Based on the "Welding Process Assessment" for the pipe section, the relevant physical and chemical properties of the girth weld were inspected to verify whether the girth weld meets the welding process requirements.

The physical and chemical properties of the girth weld were analyzed on Specimen No.4 (Specimen No.1 served as a spare). The

sample summary is listed in Table 1.

# (4) Fracture

The fracture parts of sample pipes No.2 and No.3 were sampled and analyzed. The sampling positions are shown in Fig. 5(c). Five areas (at clock positions of 12:00, 2:30, 5:30, 8:00, and 10:30) with uneven, sharp, and tearing marks were selected for sampling and analyzed by metallography and a scanning electron microscope to observe the microscopic morphology of the fracture.

## 3.2. Experimental equipment

A large number of physical and chemical experiments are involved in this study, with the following test equipment models and parameters:

ARL4460 photoelectric direct reading spectrometer was utilized for chemical composition testing. This device is typically used to determine 24 elements in steel, alloy, nickel-based alloy and other metal materials, and it can detect multiple elements at the same

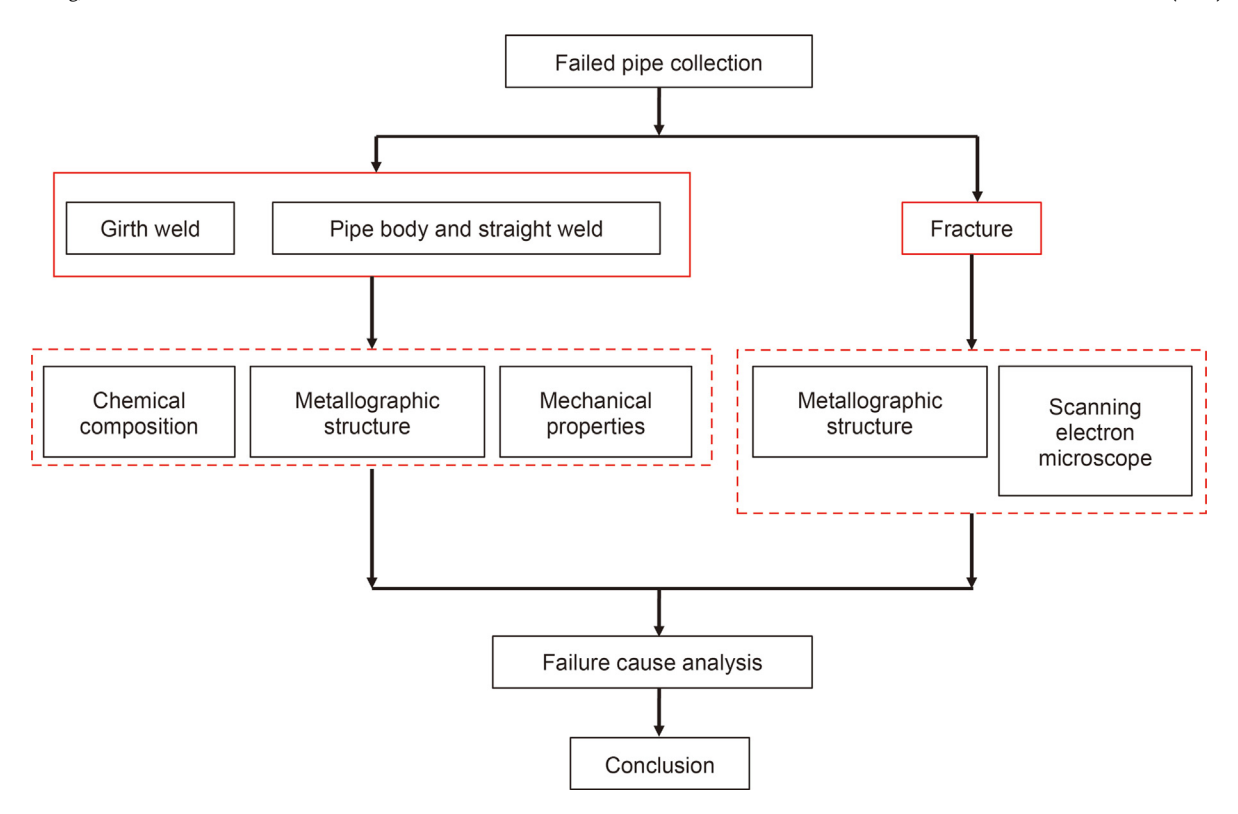


Fig. 4. Adopted experimental process.

time with high accuracy of up to 0.0001%.

An SHT 4106 mechanical testing machine with a maximum force of 1000 kN was used for the tensile properties testing.

A PIT302D impact machine with a maximum initial energy of 300 J was used for the Charpy impact energy testing.

A WZW-1000 three-cylinder bending tester with a maximum load of 1000 kN was used for the bending testing.

An OLS-4100 laser confocal microscope was utilized to observe the microstructure. This microscope offers a magnification of 50–17600 times.

A TESCAN VEGA II scanning electron microscope (SEM) was adopted to analyze the crack appearance and micro area compositions. This device has a maximum magnification of 10000 times, a resolution of 3—4 nm, and energy spectrum elements ranging from B5 to U92.

## 4. Experimental results

# 4.1. Pipe body and straight weld

#### 4.1.1. Chemical composition analysis

An ARL 4460 direct-reading spectrometer was used for chemical composition analysis. Nitrogen (N) element analysis was performed by a TC600 oxygen and nitrogen analyzer. The results are listed in Table 2. The chemical composition near the fracture is consistent with that of the unbroken pipe section and meets the requirements of Chinese standard GB/T9711.1—1997 (SAC, 1997).

# 4.1.2. Metallographic structure analysis

An OLS 4100 laser confocal microscope was employed to analyze the straight weld's metallographic structure and grain size. The metallographic structure is illustrated in Fig. 6(a), and the macroscopic appearance of the straight weld is displayed in Fig. 6(b). There were no abnormalities in the metallographic structure or

macroscopic welding defects in the straight weld.

#### 4.1.3. Bending of the straight weld

A WZW-1000 bending testing machine was utilized for the bending test, and surface bending and back bending tests were conducted on the welded seam of the pipe body. Table 3 lists the results. The bending performance meets the requirements of Chinese standard GB/T9711.1—1997 (SAC, 1997).

#### 4.1.4. Comparative analysis of mechanical properties

Tensile and Charpy impact tests were performed on the pipe samples at the fracture and unbroken parts, and the results are detailed in Table 4. The yield strength elongation and yield-to-strength ratio at the fracture site decreases, the tensile strength remains unchanged, and the Charpy impact toughness reduces significantly.

#### 4.2. Girth weld

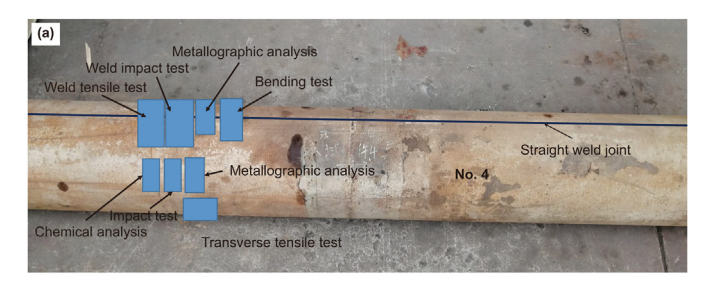
#### 4.2.1. Chemical composition analysis

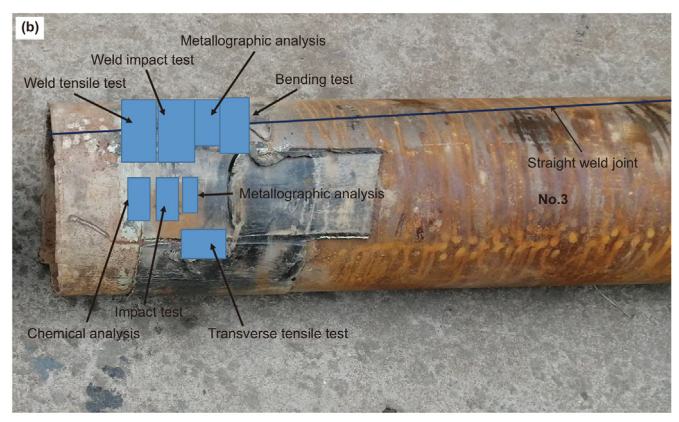
An ARL 4460 direct-reading spectrometer was used for chemical composition analysis, and the results are listed in Table 5. The chemical composition of the weld is in line with the requirements of the Welding Evaluation.

## 4.2.2. Metallographic structure analysis

An OLS 4100 laser confocal microscope was employed to analyze the microstructure, grain size, and macrostructure of the girth weld. The microstructure is shown in Fig. 7, and the macrostructure of the weld is depicted in Fig. 8. No obvious abnormalities were observed in the metallographic structure.

The macro metallography of the girth weld is that the weld cover layer and filling layer consist of 1-pass welding, and the filling layer is 2-pass welding, which meets the requirements of the





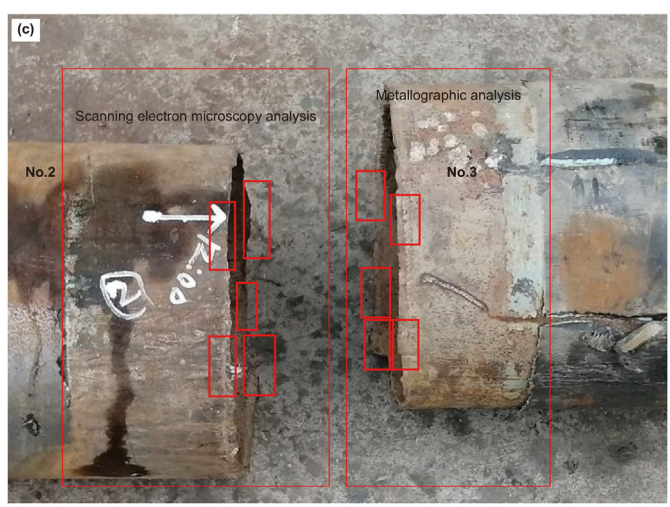


**Fig. 5.** Schematic diagram of sampling position: (**a**) sampling of physical and chemical properties of pipe body and straight seam of pipe section No.4, (**b**) sampling position of pipe body and straight weld at fracture edge of pipe section No.3, (**c**) sampling position at fracture

**Table 1**Physical and chemical properties of girth welds.

Item	Clock position	Quantity
Metallographic analysis	6:00, 9:00, 12:00, 3:00	4
Hardness	6:00, 9:00, 12:00, 3:00	4
Chemical composition analysis	6:00	1
Tensile test	6:00	2
Impact test	9:00, 3:00	12
Face bending test	1:30, 7:30	2
Back bending test	4:30, 10:30	2
Broken groove hammer test	2:30, 7:30	2

Welding Evaluation. Various degrees of misalignment are present around the entire circle, with misalignment values less than 4.5 mm, which are within the qualified range specified in the Welding Evaluation.

#### 4.2.3. Mechanical properties test

The test results of mechanical properties are detailed in Table 6. The tensile properties, Charpy impact properties, bending, and broken groove hammer all meet the requirements of the Welding Evaluation.

Table 7 compares the mechanical properties of the pipe body base material and the girth weld. This indicates that one sample is fractured in the heat-affected zone (Fig. 9), and its strength is lower than the measured value of the base material. This demonstrates that the strength matching between the girth weld and the base material in the pipe section is not uniform, revealing a localized weak matching phenomenon.

#### 4.3. Fracture

#### 4.3.1. Metallographic structure analysis

Based on Chinese standards GB/T 13298—2015 and GB/T 4335-2013, an OLS 4100 laser confocal microscope was used to analyze the metallographic structure, grain size, and macrostructure of the weld at the fracture girth. The results of the metallographic structure analysis are listed in Table 8, and the macrostructure of the weld is shown in Fig. 10. The acronyms in Table 8 are as follows: "P" represents pearlite, "PF" represents polygonal ferrite, "Bgranules" represents granular bainite, "IAF" represents intracrystalline nucleation acicular ferrite, "MA" represents martensitic austenitic island structure. No abnormalities were observed in the metallographic structure, and misalignment defects were found at positions 5:30 and 8:00.

#### 4.3.2. Scanning electron microscope detection

The SEM results of the fracture are depicted in Fig. 11. Since the pipe section was exposed to water erosion for a long time after fracturing, corrosion has occurred at the fracture site. Despite several cleanings, corrosion products cannot be removed at some fractures.

#### 5. Discussion

The physical and chemical property analysis indicates that the base material and the straight weld of the water-damaged fracture pipe section conform to the pipe-making standards. The girth welds at both the fracture and the intact parts do not exceed the standard defects, and the fracture is clearly an overload fracture. The mechanical properties of the base metal and straight welds near the fracture change.

The failure of the pipe section is attributed to the overload at the crossing center, caused by the scouring action of water flow, which leads to the tearing and destruction of the girth weld. The factors that influence the failure of this pipe section include changes in the pipeline crossing structure, the erosive action of water flow, and the incorrect edge defect of the girth weld. This study analyzes the failure process based on these three influencing factors.

#### 5.1. Changes in pipeline crossing structure

Data investigation reveals that the pipe section was originally a riverbed crossing pipe section with a buried depth of about 3–4 m. The river is a seasonal river, typically shallow and narrow. Due to prolonged rainstorms, the water level surged, and the flood erosion gradually lowered and widened the riverbed, eventually exposing the buried pipe section and altering the laying condition from the original riverbed crossing to a new riverbed crossing scenario.

The pipeline crossing structure change altered the pipe section's stress distribution. Before the flood disaster, the pipeline was buried through the riverbed, where the constraint effect of the soil

 Table 2

 Chemical composition analysis results (unit: mass fraction %).

Elements	Near the break	Unbroken pipe section	GB/T9711.1-1997 (SAC, 1997)
Carbon (C)	0.079	0.079	0.16 or less
Silicon (Si)	0.20	0.20	0.45 or less
Manganese (Mn)	1.01	1.01	1.6 or less
Phosphorus (P)	0.014	0.014	0.025 or less
Sulfur (S)	0.0041	0.0041	0.02 or less
Nitrogen (N)	0.0032	0.0031	0.012 or less

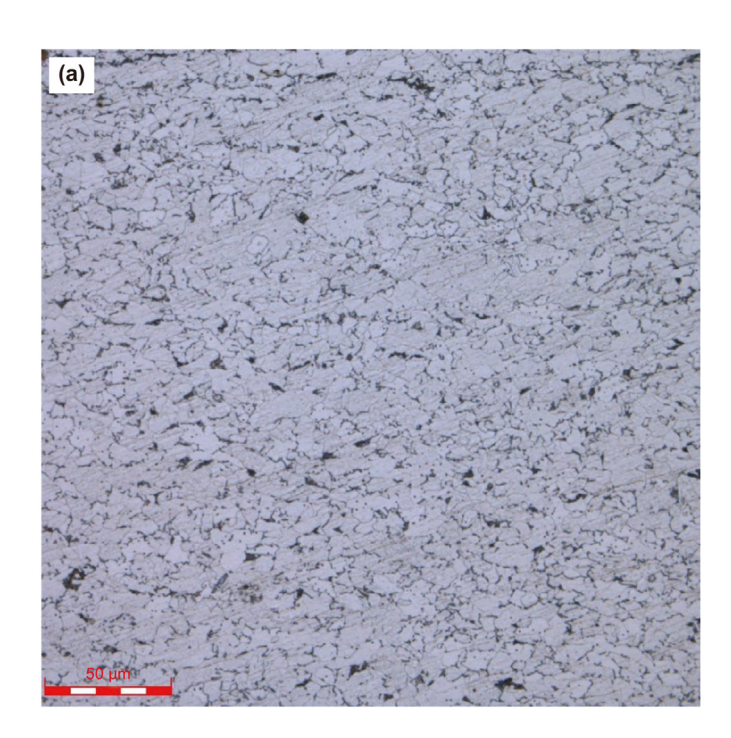




Fig. 6. Image of pipe structure: (a) metallographic structure, (b) weld macrostructure.

and pipe system maintained a static equilibrium. The forces on the pipe section were uniformly distributed, with no stress concentration. However, the flood-induced erosion of the riverbed has caused the river channel to widen and deepen, exposing the pipe section and transforming its structure into a typical double

cantilever beam structure. This new structure concentrates stress at the fixed support positions at both ends of the pipe section and the midpoint of the suspended span, as illustrated in Fig. 12.

# 5.2. Impact of water flow

During a flood, the pipeline experiences the combined effects of loads such as hydrodynamic force, buoyancy, and the resistance of the pipe body and soil foundation (Zhang et al., 2006), as depicted in Fig. 13.

Due to the scouring effect of the flood, the pipe section is subjected to cyclic bending loads, altering the pipe section's mechanical properties and structural forces.

#### 5.2.1. Changes in material properties

Throughout the flood erosion, the span pipe section undergoes periodic vertical movements under the influence of water buoyancy and its own gravity, displaying periodic changes in compressive and tensile stress at the axial midpoint stress concentration, as depicted in Fig. 14.

When the floodwaters lift the pipeline, it arches upward, with the largest bending arc at the middle of the axis and the highest stress concentration. The upper arc side of the pipe section experiences local tensile stress, while the lower arc side undergoes local compressive stress.

When the pipe sinks due to its weight and water flow fluctuations, it bends in the opposite direction, where the bending arc at the middle of the axis is the largest, and the stress concentration is also the highest. The upper arc wall of the pipe section experiences local compressive stress, while the lower arc wall undergoes local tensile stress.

This analysis indicates that under the influence of flood erosion and the pipeline's gravity, the local pipeline endures cyclic stretching and compression stresses. However, from the actual vibration process of the pipeline, it is observed that the curvature of the lifting and sinking is asymmetrical, with the sinking curvature being larger, thus subjecting the local pipeline to cyclic loads of asymmetric stress. Under the load, the material's mechanical properties are affected, and these changes manifest as a ratchet effect in strain, a Bauschinger effect in stress, and cyclic hardening in hardness.

### (1) Ratchet effect

**Table 3**The bending test results of the straight weld of the pipe body.

Items		Sample length, mm	Sample width, mm	Sample thickness, mm	Bending shaft diameter, mm	Bending angle, $^\circ$	Result
Face bending	Near the break	300	25	Full wall thickness	75	180	No cracks
	Unbroken pipe section	300	25	Full wall thickness	75	180	No cracks
Back bending	Near fracture	300	25	Full wall thickness	75	180	No cracks
	Unbroken pipe section	300	25	Full wall thickness	75	180	No cracks

 Table 4

 Comparison of mechanical properties between fractured and unbroken parts.

Items		Unbroken area	Site of fracture	Contrast
Base material	Yield strength, MPa	441	428	-2.95%
	Tensile strength, MPa	524	524	0.00%
	Bending ratio $R_{t0.5}/R_{\rm m}$	0.84	0.81	-3.57%
	Elongation, %	37.0	33.7	-8.92%
	Charpy impact, J	44.3	42.7	-3.61%
Straight weld	Tensile strength, MPa	546	546	0.00%
	Charpy impact (center of weld), J	52.7	41	-22.20%
	Charpy Shock (Heat affected zone), J	80.3	77	4.11%

**Table 5**Results of chemical composition analysis (unit: mass fraction %).

Elements	Test results	Welding Evaluation regulations
Carbon (C)	0.096	0.2 or less
Silicon (Si)	0.22	1.0 or less
Manganese (Mn)	0.68	1.2 or less

The tensile and compressive stresses of the failed pipeline are asymmetrical as it arches and sinks. When the local material stretches or compresses, it deforms. Upon unloading and reverse loading, the material initially recovers along the elastic line. Then it deforms in reverse, with the reverse load being smaller than the initial load and the reverse deformation of the material being less than the initial deformation. Hence, residual strain accumulates.

This process repeats when the pipe section is impacted by water flow, leading to the ratchet effect in the material. The ratchet effect results in cyclic accumulation of plastic strain, reducing the material's resistance to destructive strain (Paul et al., 2011a, b, c; Lin et al., 2013).

Because the ratchet effect can cause the accumulation of residual plastic deformation in materials, the initial length of the sample includes residual strain when the part affected by the ratchet effect is sampled for a tensile test. Fig. 15 indicates that the tensile sample is taken near the area affected by the ratchet effect, and the length is  $L+\Delta L$ , where  $\Delta L$  is the accumulation of deformation caused by the ratchet effect. The normal sample length should be L, and when the sample is stretched to break, the length becomes  $L_1$ . For the specimen affected by the ratchet effect, its elongation at break is significantly reduced.

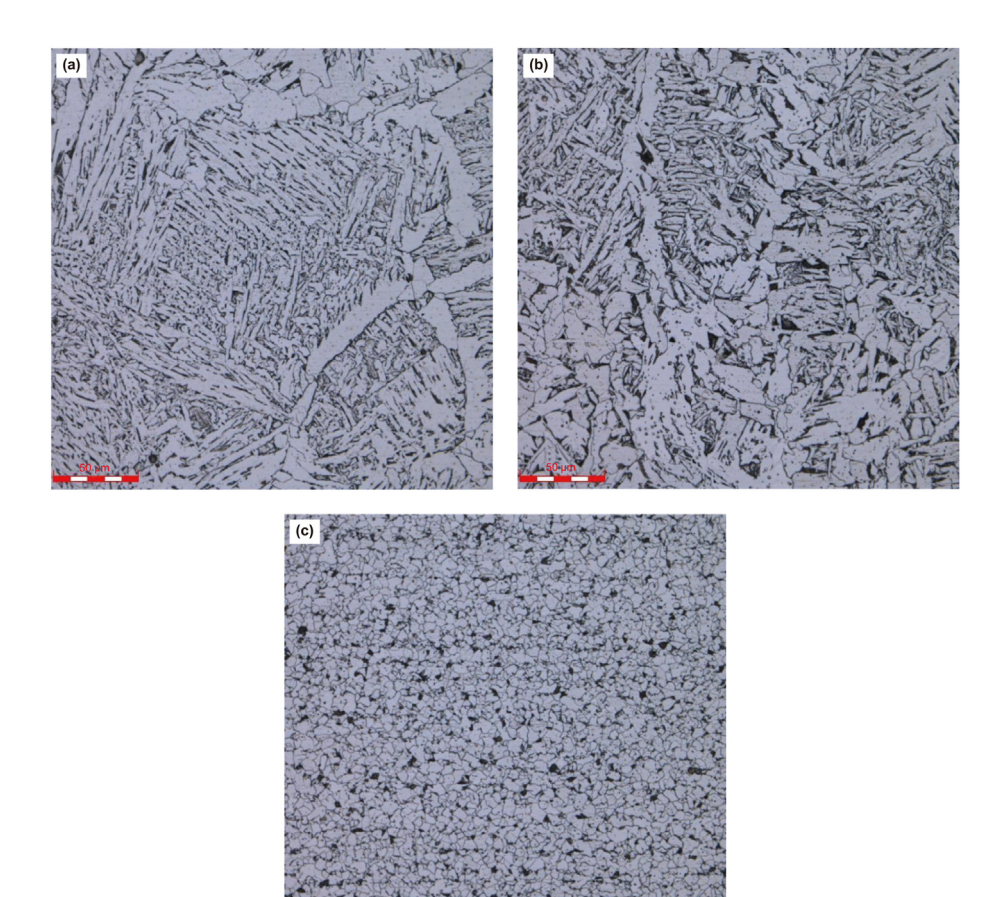


Fig. 7. Microstructure of girth weld: (a) fusion zone, (b) weld zone, (c) fine-grained zone.

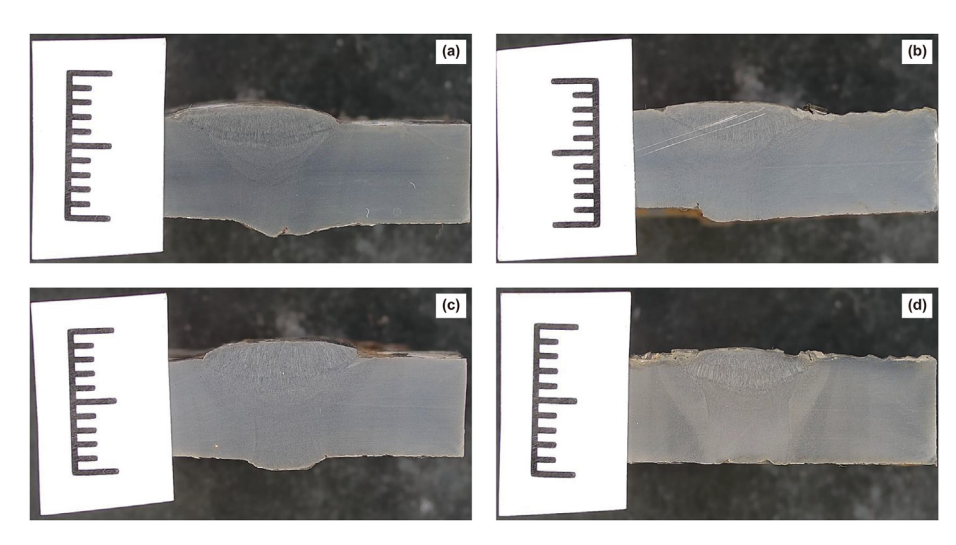


Fig. 8. Macro picture of girth weld: (a) 12:00, (b) 3:00, (c) 6:00, (d) 9:00.

**Table 6**Test results of mechanical properties of welds.

Test items			Test results	Welding review requirements
Lateral drawing	Tensile strengt	h	499 MPa 524 MPa	460-825 MPa 460-825 MPa
Charpy impact	At 3:00	Weld Heat affected zone	53, 51, 49 J 55, 106, 111 J	≥40 J ≥40 J
	At 9:00	Weld Heat affected zone	105, 37, 104 J 92, 104 , 99 J	≥40 J ≥40 J
Face bend-1 (1:30) Face bend-2 (7:30) Back bend-1 (4:30) Back bend-2 (10:30) Broken groove hammer	r 2:30		No cracks No cracks No cracks No cracks No defect was found in the fracture	No cracks No cracks No cracks No cracks
Broken groove hammer	r 7:30		No defect was found in the fracture	Ţ

**Table 7**Comparison of mechanical properties between girth weld and base material.

Test location		Girth weld	Base metal
Tensile strength, MPa	No.1 No.2	499 (off-heat affected zone) 524 (broken at base material)	524



Fig. 9. Photo of girth weld tensile specimen.

$$\delta = \frac{L_1 - (L + \Delta L)}{L + \Delta L} \tag{1}$$

For the normal sample without ratchet effect, the elongation at break should be

$$\delta_1 = \frac{L_1 - L}{L} \tag{2}$$

 Table 8

 Results of metallographic structure analysis.

Specimen	Weld	Fusion zone	Fine-grained zone
12:00	PF + IAF + B <sub>granules</sub>	B <sub>granules</sub> + PF	PF + MA
2:30	$PF + IAF + B_{granules}$	$B_{granules} + PF$	PF + MA
5:30	$IAF + PF + B_{granules}$	$PF + B_{granules}$	PF + MA
8:00	$PF + B_{granules} + P$	$B_{granules} + PF$	PF + MA
10:30	$IAF + PF + B_{granules}$	$B_{granules} + PF + WF$	PF + MA











**Fig. 10.** Metallographic picture of girth weld fracture: (**a**) at 12:00, (**b**) at 2:30, (**c**) at 5:30, (**d**) at 8:00, (**e**) at 10:30.

From the comparison of Eqs. (1) and (2), it is clear that the ratchet effect reduces the elongation at the break of the material.

It can be seen from Section 4.1.4 that the elongation at break of pipe base material away from the fracture is 37%, while the elongation at break of pipe base material near the fracture is reduced to 33.7%, repressing a total decrease of 8.92%. The pipe far from the

fracture is almost not affected by the ratchet effect. Hence it can be observed that the elongation at the break of the base material near the fracture decreases by 8.92% under the ratchet effect.

### (2) Bauschinger effect

In a series of tensile and compression experiments on steel conducted by Bauschinger (1881), the yield point of the material decreased during reverse deformation, i.e., after experiencing a certain amount of one-way tensile or compressive plastic deformation followed by reverse loading, the yield stress of the material was lower than the yield stress of continuous forward deformation. This phenomenon, known as the Bauschinger effect (Xie et al., 2019; Guo et al., 2020; Wang et al., 2020), is illustrated in Fig. 16. Under the impact of water flow, the midpoint of the suspended span section of this failed pipe section repeatedly experiences the Bauschinger effect.

Section 4.1.4 indicates that the yield strength of the pipe base material away from the fracture is 441 MPa. In contrast, the yield strength of pipe base metal near the fracture is reduced to 428 MPa, which represents a total decrease of 2.95%. The yield strength of the pipe base material away from the fracture is almost not affected by the Baushenge effect. Therefore, it can be observed that the yield strength of pipe base material near the fracture is reduced by 2.95% under the influence of the Baushenge effect.

#### (3) Cyclic hardening

The pipe body near the fracture girth weld is subjected to repeated tensile and compressive loads, causing the material to undergo plastic deformation. Due to this repeated plastic deformation, the plastic flow characteristics of the pipe body material change, leading to enhanced resistance to deformation of the material, a phenomenon known as cyclic hardening (Guo et al. 2013; Krolo et al., 2016; Wang et al., 2020). Cyclic hardening results in the deterioration of material toughness. The impact toughness of the base material near the fracture girth weld decreases by 3.61%, and that of the straight weld decreases by 22.2% compared to that of the unbroken part.

# 5.2.2. Structural resonance effect

After exposure, the pipeline becomes a double cantilever beam structure anchored on both sides of the riverbed, with the central part suspended. Under the impact of water flow and its own gravity, the pipe section vibrates, and structural vibration ultimately leads to the fracture of the pipeline. When the vibration frequency caused by the impact of water flow and the gravity of the pipe itself reaches the natural frequency of the pipe structure, the pipe section resonates, and the intense vibration causes the fracture of the girth weld at the axial midpoint of the pipe section (Choi and Haun, 1994).

When the suspended span pipe is regarded as a steel structure, its inherent natural vibration frequency is expressed by  $f_e$  (Lu et al., 2002); there is

$$f_{\rm e} = \frac{0.7K^2}{2\pi L^2} \sqrt{\frac{EI}{m_{\rm S}}} \tag{3}$$

where

 $f_{\rm e}$  is the natural frequency of the suspended pipe section in Hz; K is the coefficient describing the different end support conditions,  $K^2$  is 22 under fixed support conditions, and  $K^2$  is 9.9 under simple support conditions;

*L* is the length of the pipe span in m;

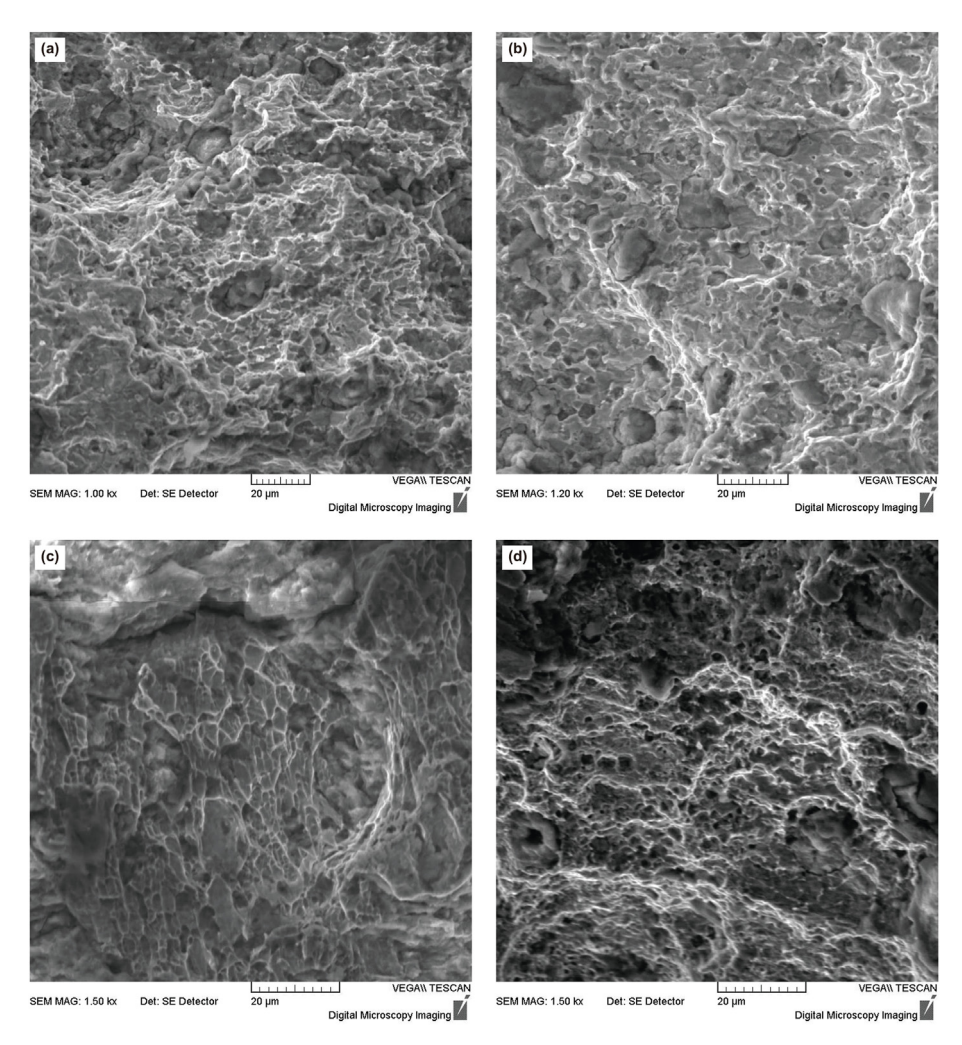


Fig. 11. Typical micromorphology of fracture specimen surface: (a) at 12:00, (b) at 2:30, (c) at 5:30, (d) at 8:00.

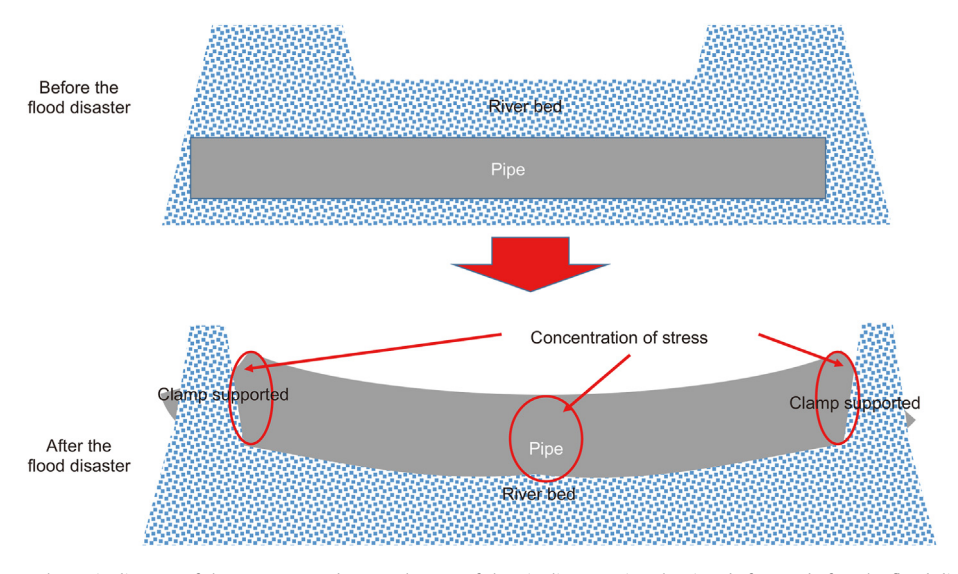


Fig. 12. Schematic diagram of the structure and stress changes of the pipeline crossing the river before and after the flood disaster.

 $m_{\rm S}$  is mass per unit length across the pipe; EI is the bending stiffness of the pipe span. The natural frequency of the pipe section is calculated to be

approximately 18.89 Hz, indicating that the vibration amplitude of the pipe section is most intense when the vibration frequency generated by the water flow is about 18.89 Hz, ultimately leading to

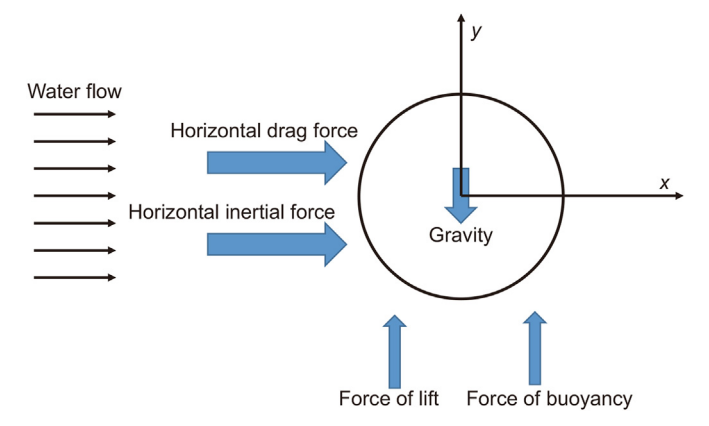


Fig. 13. Schematic diagram of load-bearing condition of flood pipeline.

the fracture of the annular weld near the axial midpoint.

#### 5.3. Misalignment defect of girth weld

Based on the results of metallographic observation, both the unbroken and broken girth welds of the pipe section have misalignment defects. According to the provisions of Welding Evaluation, these edge defects do not exceed the standard.

However, the Welding Evaluation is conducted under conventional service conditions, and the water damage conditions are extreme natural disaster conditions. The number of misalignment defects deemed acceptable by the Welding Evaluation can be invalidated due to flooding.

This study utilizes ABAQUS simulation to illustrate the influence of misalignment on the stress distribution of girth welds. The model replicates the same pipe as that studied herein, with an external diameter of 237 mm, a wall thickness of 7 mm, and an internal pressure of 4 MPa. The normal weld and the weld with misalignment were simulated, respectively, and the amount of misalignment was set to 2 mm. The simulation results are shown in Fig. 17(a) and (b). It can be seen that, compared to the normal weld, the weld with misalignment will have obvious stress concentration at the toe of the weld, which is consistent with the simulation results in the literature (Li et al., 2021) (as shown in Fig. 17(c)).

Stress relaxation occurred on the side with a higher position, and the stress level was significantly lower than the stress at the far end. Under the impact of flood, the pipeline vibrates, the girth weld near the axial midpoint of the pipeline experiences cyclic compression and tensile load, and the stress concentration at the weld toe of the misalignment side intensifies, resulting in the girth weld cracking from the misalignment side, the crack extending around the girth weld, and finally the complete fracture.

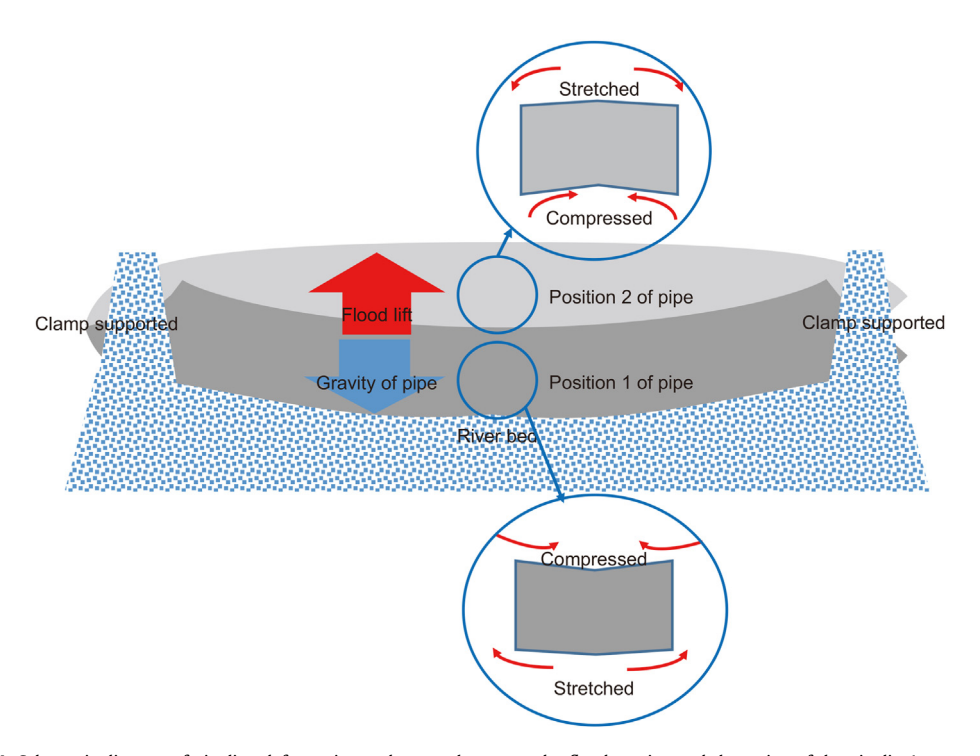


Fig. 14. Schematic diagram of pipeline deformation and stress changes under flood erosion and the action of the pipeline's own gravity.

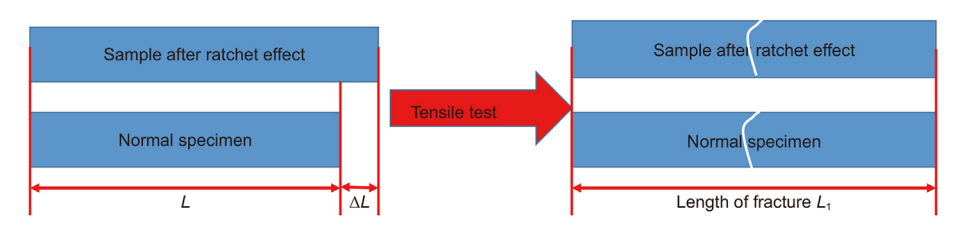


Fig. 15. Schematic diagram of failure strain reduction caused by the ratchet effect.

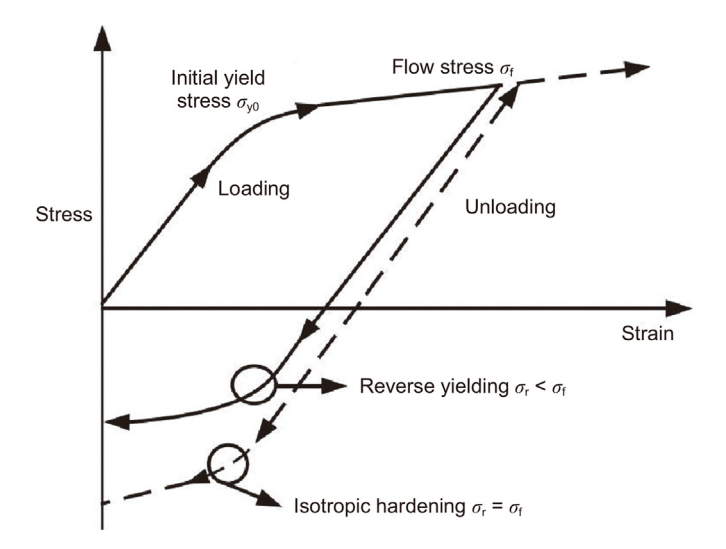


Fig. 16. The stress-strain diagram of the Bauschinger effect.

#### 5.4. Analysis of the pipe section failure process

The above analysis shows that the water pipe section failed due to various interacting factors. The main failure process is as follows: flood-induced water and soil erosion expose the pipeline on the riverbed, changing its status from a buried to a suspended crossing. The suspended pipeline vibrates due to its weight and flood impact. This vibration induces a reciprocating cyclic load of stretching and compression near the axial midpoint of the pipe. Under the ratchet effect, the elongation at the break of the material decreases; under the Bauschinger effect, both the yield strength and yield ratio decrease. Cyclic hardening further reduces the impact of the toughness of the material. Calculations show that the natural frequency of the suspended span pipe structure is approximately 18.89 Hz. At this frequency, the vibration amplitude of the pipe section is most intense, eventually causing the annulus weld near the axial midpoint to break. The failure process is illustrated in Fig. 18.

The metallographic diagram of the girth weld at the fracture shows that the fracture initially cracks at the weld toe of the cover layer on one side of the girth weld between 11:30 and 12:30 under vibration. The crack then progressively penetrates the weld along

the heat-affected zone. In the clockwise direction, as the clock position increases, the crack expands from one side of the heat-affected zone to the center of the weld and spreads to the opposite side of the heat-affected zone around 6:00. The stress concentration shifts and the crack distribution within the wall thickness also develops from one side of the heat affected zone to the other. In contrast, as the clock position decreases, the crack extends along one side of the heat-affected zone in the counter-clockwise direction and finally into the base material. When the crack reaches about 6:00, it fully enters the base material. The cracks from both directions intersect at 6:00. Due to the incomplete alignment of the two crack paths, there are only a few connections within the pipe body at 6:00, which eventually tear apart and break under the stress of vibration, resulting in a step-like fracture. The fracture process is depicted in Fig. 19.

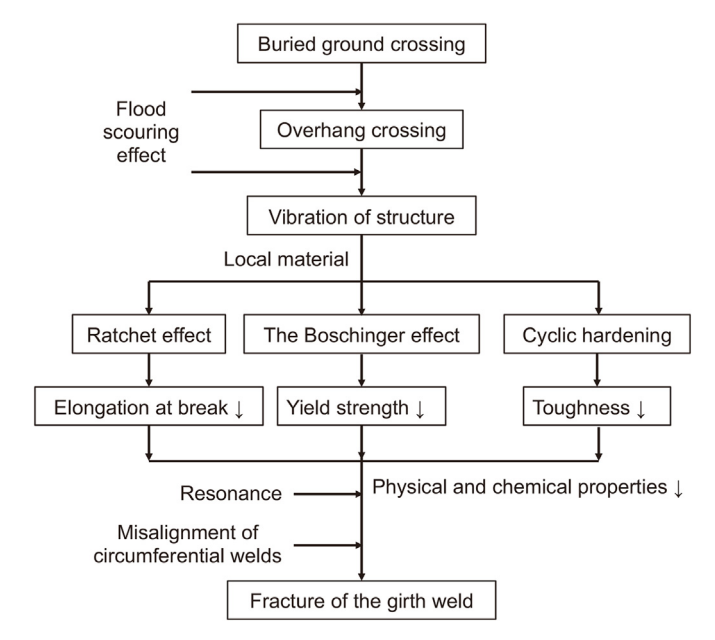


Fig. 18. Schematic diagram of pipeline fracture process.

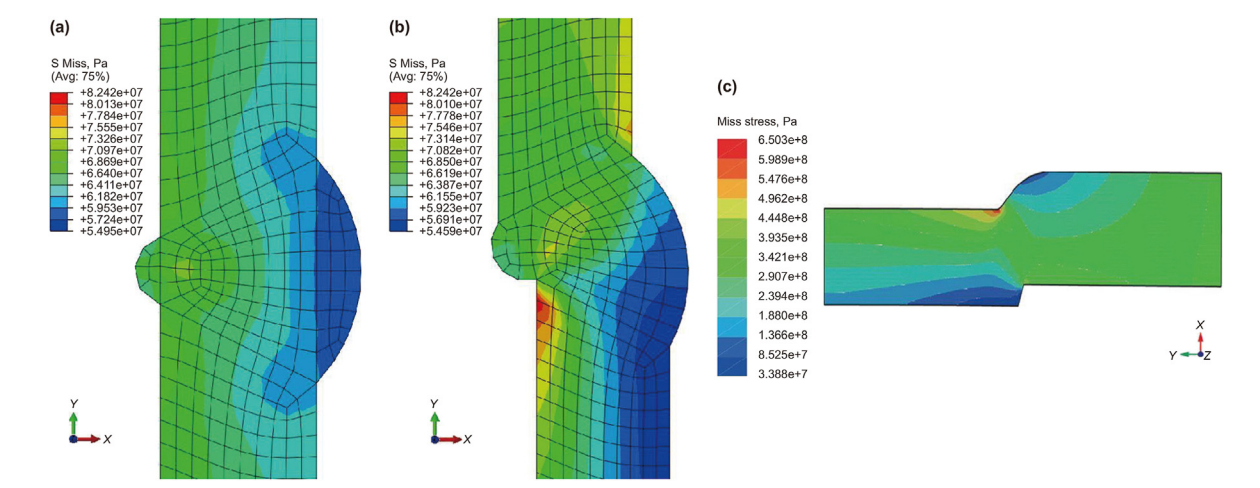


Fig. 17. Stress concentration of the girth weld caused by the misalignment: (a) normal girth weld, (b) girth welds with misalignment, (c) simulation results of girth welds with misalignment in the literature (Li et al., 2021).

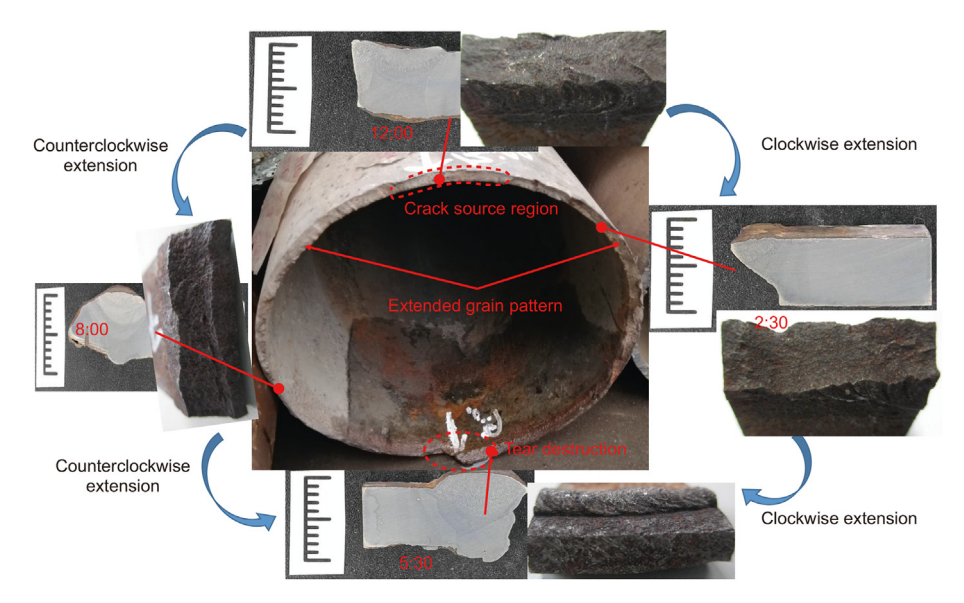


Fig. 19. Schematic diagram of the fracture process of the pipeline.

#### 6. Conclusion

In the context of a specific water pipeline failure incident, this study delves into the microstructural and chemical attributes of the samples. The mechanisms of deformation failure and the root causes of pipeline failures resulting from water flow in practical engineering scenarios are scientifically investigated. The intricate interplay between hydrodynamic forces and pipeline material characteristics is elucidated, thereby offering a scientifically valuable case study for the analysis of water pipeline failures. The main conclusions are as follows:

- (1) The physical and chemical properties of the pipe base metal and the welds are in line with Chinese standard GB/T 9711.1—1997, but that of the pipeline materials close to the fracture and away from the fracture differ, indicating that the performance of the batch of pipelines meets the requirements of the standard during construction. Nevertheless, the performance of the pipeline materials changes under the impact of water flow.
- (2) The severe vibration with a frequency of approximately 18.98 Hz is the direct cause of the fracture of the girth weld at the axial midpoint of the pipe section. Under the vibration caused by the water impulse, the material near the axial midpoint of the pipe section suffers the ratchet effect, resulting in an 8.92% decrease in elongation at break. Additionally, it causes the Bauschinger effect, leading to a yield strength reduction of 2.95%, and induces the cyclic hardening effect, that results in a reduction of 22.2% in the impact toughness of the weld. The stress concentration at the toe of the girth weld caused by the misalignment is also one of the reasons for the fracture.
- (3) The fracture process of the girth weld is as follows: under the interaction between the flood shock vibration load and its gravity, due to the weak matching phenomenon, great stress concentration leads to cracking at the outer wall welding toe near the 12:00 position. Under the condition of ratchet effect, the crack gradually expands to the 6:00 position and finally fails with ductile tear failure.

#### **CRediT authorship contribution statement**

**Hai-Liang Nie:** Writing — original draft, Conceptualization. **Zhi-Yong Wang:** Writing — review & editing, Investigation. **Chen Chen:** Formal analysis. **Wei Dang:** Methodology. **Sen Zhao:** Investigation. **Jun-Jie Ren:** Formal analysis. **Xiao-Bin Liang:** Validation. **Ke Wang:** Software. **Wei-Feng Ma:** Writing — review & editing.

# **Declaration of competing interest**

The authors declare that they have no known competing financial interests or personal relationships that could have appeared to influence the work reported in this paper.

# Acknowledgments

This work was supported by the Youth Science and Technology New Star Project of Shaanxi Province (grants Nos. 2024ZC-KJXX-002, 2021KJXX65 and 2023KJXX-092), the Natural Science Foundation of Shaanxi Province (grant No. 2021JQ-947), and the Basic Research and Strategic Reserve Technology Research Fund of the China National Petroleum Corporation (projects Nos. 2022DQ03-05 and 2023DQ03-07).

#### References

Bauschinger, J., 1881. Changes of the elastic limit and the modulus of elasticity on various metals. Zivilingenieur 27, 289–348.

- Choi, H.S., Haun, R.D., 1994. The effect of residual tension and free span-induced moments on vortex shedding of deep water pipelines. Forth International Offshore and Polar Engineering Conference.
- Guo, Y., Luo, Y.R., Wang, Q., 2013. Mean strain effect on the cyclic stress-strain behavior of steel structure materials Q235. Adv. Mater. Res. 602, 430–434. https://doi.org/10.4028/www.scientific.net/AMR.602-604.43.
- Guo, Y.B., Ho, H.C., Chung, K.F., Elghazouli, A.Y., 2020. Cyclic deformation characteristics of S355 and S690 steels under different loading protocols. Eng. Struct. 221, 111093. https://doi.org/10.1016/j.engstruct.2020.111093.
- Hale, J.R., Lammert, W.F., Allen, D.W., 1991. Pipeline on-bottom stability calculations: comparison of two state-of-the-art methods and pipe-soil model verification. Proc.l2th Offshore Technology Conference. https://doi.org/10.4043/6761-MS.
- Krolo, P., Grandić, D., Smolčić, Ž., 2016. Experimental and numerical study of mild steel behaviour under cyclic loading with variable strain ranges. Adv. Mater. Sci. Eng. 1–3. https://doi.org/10.1155/2016/7863010.
- Lin, Y.C., Zheng, H.L., Xiao, M.C., Jian, C., 2013. Uniaxial ratcheting and fatigue failure behaviors of hot-rolled AZ31B magnesium alloy under asymmetrical cyclic

- stress-controlled loadings. Mat. Sci. Eng. A-Struct. 573, 234-244. https:// doi.org/10.1016/j.msea.2013.03.004.
- Li, Z.W., Wu, M.C., Wang, X.Y., Fan, Y.R., et al., 2021. Stress concentration test and simulation of girth weld with misalignment based on wide plate tensile test. Oil Gas Storage Transp. 40 (2), 178–184. https://doi.org/10.6047/j.issn.1000-8241.2021.02.009 (in Chinese).
  Lu, X.G., Tang, Y.G., Zhang, Z.G., 2002. A new method for calculation of natural frequency of suspended pipeline. Trans. Tianjin Univ. 8 (2), 282–284.
- Paul, S.K., Siyaprasad, S., Dhar, S., Tarafder, S., 2011a, Key issues in cyclic plastic deformation: experimentation. Mech. Mater. 43 (11), 705-725. https://doi.org/ 10.1016/i.mechmat.2011.07.011.
- Paul, S.K., Sivaprasad, S., Dhar, S., Tarafder, S., 2011b. Cyclic plastic deformation and damage in 304LN stainless steel. Mat. Sci. Eng. A-Struct. 528 (15), 4873-4882. https://doi.org/10.1016/j.msea.2011.03.048.
- Paul, S.K., Sivaprasad, S., Dhar, S., Tarafder, S., 2011c. Cyclic plastic deformation behavior in SA333 Gr. 6 C-Mn steel. Mat. Sci. Eng. A-Struct. 528 (24), 7341–7349. https://doi.org/10.1016/j.msea.2011.06.009.
- SAC. Petroleum and Natural Gas Industries-Steel Pipe for Pipelines-Technical

- Deivery Conditions-Part 1: Pipes of Requirement Class A. Chinese Standard: GB/T 9711.1-1997, published 03-11-1997 (in Chinese).
- Wang, C., Fan, J.S., Xu, L.Y., Nie, X., 2020. Cyclic hardening and softening behavior of the low yield point steel: implementation and validation. Eng. Struct. 210, 110220. https://doi.org/10.1016/j.engstruct.2020.110220.
- Xian, Z.W., 2002. Underwater crossing accident of large oil and gas pipeline and its protection. Natural Gas and Oil 20 (2), 7–9. https://doi.org/10.3969/j.issn.1006-5539.2002.02.003 (in Chinese).
- Xie, X.F., Jiang, W., Chen, J., Zhang, X., Tu, S.T., 2019. Cyclic hardening/softening behavior of 316L stainless steel at elevated temperature including strain-rate and strain-range dependence: experimental and damage-coupled constitutive modeling. Int. J. Plast. 114, 196–214. https://doi.org/10.1016/j.ijplas.2018.11.001.
- Zhang, L.J., Wang, H., Guo, J., 2015. Causes of water damage accident in the Shiting River crossing section of Lancheng pipeline. Oil Gas Storage Transp. 34 (12), 1351–1354. https://doi.org/10.6047/j.issn.1000-8241.2015.12.020 (in Chinese).
- Zhang, L.T., Liu, Y., Wei, L.X., et al., 2006. Simulation and analysis of impacted pipe. Pipeline Technology and Equipment (2), 11–13. https://doi.org/10.3969/ j.issn.1004-9614.2006.02.004 (in Chinese).